Nano Research 2014, 7(7): 1073–1082
DOI 10.1007/s12274-014-0470-7
Research Article
ISSN 1998-0124
CN 11-5974/O4

Ultralong-life and high-rate web-like $Li_4Ti_5O_{12}$ anode for high-performance flexible lithium-ion batteries

Xianfu Wang[1,2], Bin Liu[2], Xiaojuan Hou[2], Qiufan Wang[2], Wenwu Li[2], Di Chen[2], and Guozhen Shen[1] (✉)

[1] *State Key Laboratory for Superlattices and Microstructures, Institution of Semiconductors, Chinese Academy of Science, Beijing 100083, China*

[2] *Wuhan National Laboratory for Optoelectronics (WNLO) and School of Optical and Electronic Information, Huazhong University of Science and Technology (HUST), Wuhan 430074, China*

Received: 19 February 2014
Revised: 1 April 2014
Accepted: 3 April 2014

KEYWORDS
ultralong-life,
high-rate,
web-like $Li_4Ti_5O_{12}$ anode,
flexible batteries

ABSTRACT

Flexible lithium ion batteries (LIBs) have recently attracted increasing attention as they show unique promising advantages, such as flexibility, shape diversity, and light weight. Similar to conventional LIBs, flexible LIBs with long cycle life and high-rate performance are very important for applications of high performance flexible electronics. Herein, we report a three-dimensional (3D) web-like binder-free $Li_4Ti_5O_{12}$ (LTO) anode assembled from numerous 1D nanowires exhibiting excellent cycling performance with high capacities of 153 and 115 mA·h·g^{-1} after 5,000 cycles at 2 C and 20 C, respectively, and excellent rate property with a capacity of 103 mA·h·g^{-1} even at a very high current rate of 80 C. Surprisingly, a flexible full battery assembled from the web-like LTO nanostructure and $LiMn_2O_4$ (LMO) nanorods exhibited a high capacity of 125 mA·h·g^{-1} at high current rate of 20 C, and showed excellent flexibility with little performance degradation even in seriously bent states.

1 Introduction

The design of flexible and portable electronic systems, such as rollup displays, smart cards, wireless sensors, and wearable devices, requires flexible, and environmentally friendly energy storage devices with shape-conformability, aesthetic diversity and excellent mechanical properties [1–6]. As one type of flexible power source, flexible lithium ion batteries (LIBs) have drawn great interest, and recently, many devices based on conductive paper [7, 8], three-dimensional electrodes [9, 10], and cable-type structures [11–15] have been successfully fabricated. Similar to conventional LIBs, flexible LIBs with high safety, long cycle life and high-rate performance are very important for applications of high performance flexible electronics. To meet the high-rate and long-life requirements, many strategies have been developed, such as reducing the transport path lengths of lithium ions and electrons [16–18], increasing the lithium diffusion coefficient [19], improving the electronic conductivity [20, 21], and enhancing the active surface between electrode

Address correspondence to gzshen@semi.ac.cn

materials and the electrolyte [22–24]. Nevertheless, the state-of-the-art electrodes, especially for the flexible LIB systems, still suffer from short cycle life and insufficient rate performance. Fabricating novel structured electrodes with ultralong-life and high-rate performance is still strongly desirable for flexible batteries.

Spinel lithium titanate $Li_4Ti_5O_{12}$ (LTO) has been regarded as one of the most promising anode materials for long-life and high-rate LIBs because of its zero volume change during lithiation and the improved safety owing to an extremely flat discharge and charge plateaus at about 1.55 V vs. Li/Li^+, which make it safe by avoiding the formation of a solid-electrolyte interphase (SEI) [25–30]. However, the kinetic problems associated with low electrical conductivity (10^{-13} S·cm^{-1}) and lithium diffusion coefficient (10^{-9} to 10^{-13} cm^2·S^{-1}) indicate that only a limited area of the outer surface layer is available for Li^+ insertion/extraction, especially at high charge–discharge rates [25, 31]. As a result, a great deal of effort has been devoted to the synthesis of LTO nanostructures with large surface area and reduced size, such as nanowires and nanosheets, to enhance the active sites for Li^+ insertion/extraction [25–28]. Benefiting from their kinetically favorable structures, these nanostructures have indeed exhibited significantly improved rate capability and prolonged cycle life. In addition, binder-free and self-supported LTO nanostructures on carbon fabric and titanium (Ti) foil have been demonstrated with ultrafast power rate and long lifespan because of the enhanced active surface and electrochemical environment for lithium storage reactions [27, 28]. However, charge–discharge cycling of such LTO anodes for more than 5,000 times has seldom been attained, and their applications in flexible batteries still need to be further developed.

In this work, we have designed a three-dimensional (3D) web-like LTO electrode assembled from numerous 1D nanowires grown directly on Ti foil by using a facile template-free route. When used as a binder-free anode for LIBs, the as-synthesized web-like LTO nanostructure manifest excellent cycling performance with high capacities of 153 and 115 mA·h·g^{-1} after 5,000 cycles at 2 C and 20 C, respectively, and excellent rate properties with capacity of 103 mA·h·g^{-1} even at a very high current rate of 80 C (1 C rate is taken to be 175 mA·g^{-1}) due to the enhanced active surface, and the reduced transport path lengths of lithium ions and electrons. Excitingly, a flexible full battery assembled from the web-like LTO nanostructure and $LiMn_2O_4$ (LMO) nanorods exhibited a high capacity of 125 mA·h·g^{-1} at high current rate of 20 C. More importantly, the as-fabricated full battery showed excellent flexibility with little performance degradation even when it was bent to a radius of < 8 mm. The realization of this flexible battery with high-rate performance will benefit the development of flexible electronics.

2 Experimental

2.1 Synthesis and characterization of web-like $Li_4Ti_5O_{12}$ nanostructures on Ti foil

The web-like $Li_4Ti_5O_{12}$ nanostructures were synthesized via a modified hydrothermal method, similar to the previous report [26]. In a typical process, a piece of Ti foil (5 × 1 cm) was ultrasonically cleaned in water, acetone and ethanol for 15 min, and then placed in a 50 mL Teflon-lined stainless steel autoclave which was filled with 40 mL of 1 M NaOH aqueous solution and then kept at 220 ℃ for 16 h. After hydrothermal growth, the Ti foil covered sample was immersed in 0.5 M HCl solution for 1 h to replace Na^+ with H^+, which was followed with immersion in 2 M LiOH solution at 60 ℃ for 8 h. After rinsing with deionized water and drying under ambient conditions, the Ti foil covered with white product was calcined in N_2 at a temperature of 600 ℃ for 1.5 h to obtain the LTO phase. The loading density of LTO was calculated to be 0.8 mg·cm^{-2} by carefully measuring the total weights of the Ti foil before and after the growth of LTO.

2.2 Fabrication of $LiMn_2O_4$ nanorods

$LiMn_2O_4$ nanorods were fabricated via a solid state reaction between β-MnO_2 nanorods and lithium hydroxide according to our previous report [19]. Typically, β-MnO_2 nanorods were first synthesized using a simple hydrothermal method with manganese sulfate and potassium chlorate as the reaction materials. Then the as-obtained β-MnO_2 nanorods were mixed with lithium hydroxide with molar ratio of 1:0.55,

followed by annealing at 750 ℃ for 10 h in air to obtain the $LiMn_2O_4$ nanorods.

2.3 Materials characterization

The crystal structure of the obtained samples was characterized by X-ray diffraction (XRD) (X'Pert PRO) with Cu Kα radiation. The microstructural properties were characterized using transmission electron microscopy (TEM) (Tecnai G2 F30), and scanning electron microscopy (SEM, Sirion 200). The X-ray photoelectron spectroscopy (XPS) analysis was performed on a AXIS-ULTRA DLD-600W system with a monochromatic aluminium anode X-ray source.

2.4 Electrochemical measurements

Electrochemical characterization of the half cells were was performed in laboratory-made two-electrode CR2032 coin cells assembled in an argon-filled glovebox using a pure lithium foil as the counter electrode. The conventional binder-enriched electrode was prepared by mixing 70 wt.% active material (LTO nanowires), 20 wt.% carbon black, and 10 wt.% polyvinylidene fluoride (PVDF) in N-methyl pyrrolidinone (NMP). The slurry was then spread uniformly on a Cu foil current collector and dried under vacuum at 110 ℃ for 12 h. A separator membrane (Celgard 2300) was used to isolate the two electrodes. The electrolyte was 1 M $LiPF_6$ dissolved in a mixture of ethylene carbonate (EC) and dimethyl carbonate (DMC) (v/v = 1:1). The coin cells were discharged/charged at different current densities with potential window of 1.0 – –2.5 V (vs. Li^+/Li) for the $Li_4Ti_5O_{12}$ anode (1 C = 175 mA·g^{-1}) and 3.2 – –4.5 V (vs. Li^+/Li) for the $LiMn_2O_4$ cathode (1 C = 145 mA·g^{-1}) by using a battery testing system (LAND, China). Cyclic voltammetry (CV) was measured on an electrochemical workstation (CHI 760D, CH Instruments Inc., Shanghai) at a scan rate of 0.5 mV·s^{-1}. For the full battery, each electrode was cut into a rectangle of 3 × 1 cm with a narrow strip on edge to connect with wires. The electrodes and separator were immersed in electrolyte for 12 h before the whole battery was assembled and sealed by poly(dimethyl siloxane) (PDMS) gel. The capacities and C-rate currents were calculated based on the anode active material (1 C corresponding to 175 mA·g^{-1}). The calculation of the capacities for both the half-cell and full-cell were based on the mass of the LTO.

PDMS gel was fabricated by vigorously mixing base and curing agent (Sylgard 184; Dow Corning), followed by degassing in a freezer at a temperature of 4 ℃ for 1 h and thermally curing at 50 ℃ for 3 h.

3 Results and discussion

3.1 Structural characterization

Figure 1(a) shows a photograph of a Ti foil with size of 5 × 1 cm. After reaction, the titanium foil was uniformly covered with a white product. The material grown on the Ti foil with excellent flexibility (Fig. 1(b)) can be directly used as a binder-free electrode for LIBs. The XRD pattern of the material on Ti foil is given in Fig. 1(c). All the peaks in this pattern (except those marked with # coming from the Ti substrate) can be assigned to a spinel LTO phase (JCPDS No. 049-0207). The high-resolution O 1s and Ti 2p core level XPS spectra are shown in Fig. S1 (in the Electronic Supplementary Material (ESM)). One peak centered at 530.0 eV in the O 1s spectrum can be ascribed to the Ti–O bonds, and two broad peaks centered at 464.4 and 458.9 eV correspond well with the characteristic Ti $2p_{1/2}$ and Ti $2p_{3/2}$ peaks of Ti^{4+} [32–34], revealing the purity of the as-synthesized LTO material.

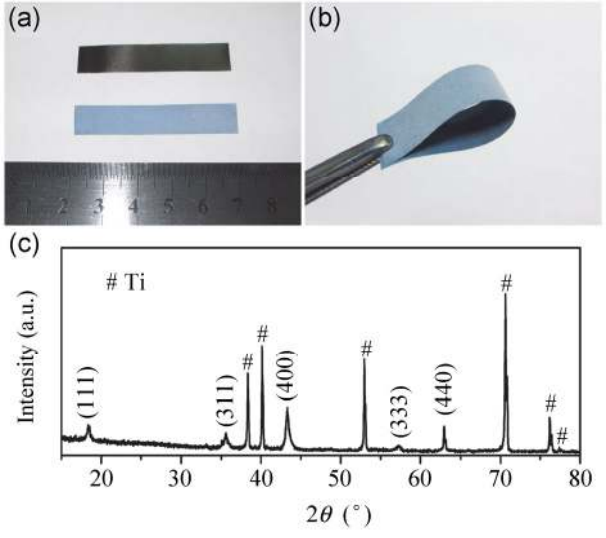

Figure 1 (a) Photographs of the titanium foil (5 × 1 cm) before and after the reaction and (b) the excellent flexibility. (c) XRD pattern of the as-synthesized LTO nanostructures on Ti foil.

A low-magnification field-emission scanning electron microscope (FESEM) image of the LTO material is shown in Fig. 2(a). It is observed that a 3D web-like architecture consisting of many wire-like nanostructures with length of about 20 μm are formed on the Ti foil. The higher magnification image in Fig. 2(b) reveals that the architecture is assembled from numerous nanowires with uniform diameters, which may increase the effective surface area, providing more active sites for electrochemical reactions. In addition, the large open space between neighboring nanowires should allow facile electrolyte diffusion throughout the thin film electrode. A TEM image of the LTO nanowires is depicted in Fig. 2(c), where a diameter of about 50 nm can be observed. A lattice spacing of 0.48 nm was seen from the High-resolution TEM (HRTEM) image (Fig. 2(d)), in good agreement with the d-spacing of 0.48 nm associated with the (111) direction of the spinel LTO structure, corresponding well with the XRD result. The 3D web-like LTO architecture on Ti foil possesses large available electrochemical active surface and shortened paths for fast ion diffusion and electronic transportation [35]. Thus, they can be directly used as a binder-free electrode for LIBs to enhance the electrochemical performance for lithium storage.

3.2 Ultralong-life and high-rate performance

In order to show that the binder-free 3D architecture offers long-life and high-rate lithium storage, a coin-type cell configuration was first used to evaluate the electrochemical properties of the as-grown LTO nanostructures on Ti foil. The long cycle performance of the binder-free anode was performed at current rates of 2 C and 20 C and the results are shown in Fig. 3(a). After 5,000 charge–discharge cycles, the discharge capacities of the web-like anode were found to be 153 and 115 mA·h·g^{-1} at 2 C and 20 C, corresponding to a small capacity loss of 12% and 17%, respectively. In contrast, for the conventional binder-enriched LTO nanowires on Cu foil, the discharge capacity decreases sharply after 500 cycles and is only 33 mA·h·g^{-1} after 2,000 cycles at a current rate of 2 C (also shown in Fig. 3(a)). The results demonstrate that the 3D web-like binder-free LTO architecture effectively enhances lithium-ion storage capacity and cycling stability. To our knowledge, this is the first report of an LTO-based flexible electrode with ultralong cycle life up to 5,000 times. The charge–discharge profiles of the web-like anode in the voltage range of 1.0–2.5 V at current rate of 2 C are also demonstrated in Fig. 3(b). The electrode achieved a first discharge capacity as high as 173 mA·h·g^{-1}, which is very close to the theoretical capacity of 175 mA·h·g^{-1}. In addition, the electrode showed a flat voltage plateau at the potential of 1.55 V ascribable to the redox of Ti^{4+}/Ti^{3+}, even after 5,000 charge–discharge cycles, revealing its excellent cycling stability.

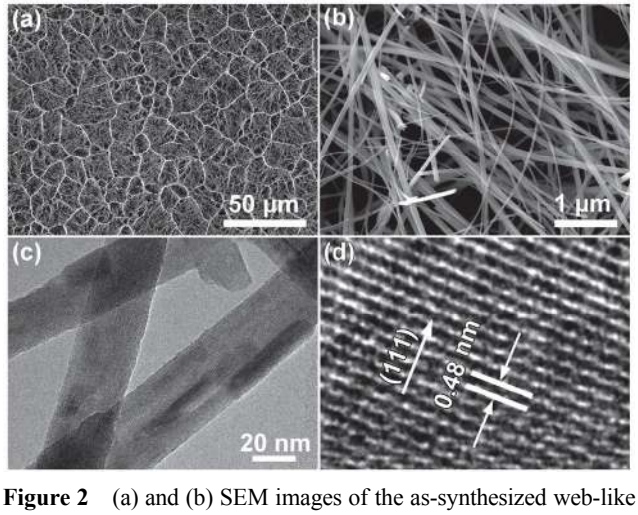

Figure 2 (a) and (b) SEM images of the as-synthesized web-like LTO nanostructures assembled from nanowires. (c) TEM and (d) HRTEM image of the LTO nanowires.

Figure 3(c) shows the discharge profiles of the web-like LTO anode at different current rates from 1 to 80 C. As can be seen, at a low C rate of 1 C, the electrode achieved a first discharge capacity as high as 180 mA·h·g^{-1}, which is a little higher than the theoretical capacity of LTO (175 mA·h·g^{-1}) because of the enhanced active surface and improved electrochemical activity. [27] As the current rate increased, the discharge capacity decreased slightly, and even at high rate of 80 C, the anode still retains a capacity as high as about 103 mA·h·g^{-1}, indicating the excellent rate capability of the LTO material. Benefiting from its unique web-like structure assembled from 1D nanowires, the binder-free LTO anode exhibits exceptional cycling response and enhanced rate capability to continuously varied current rates when compared

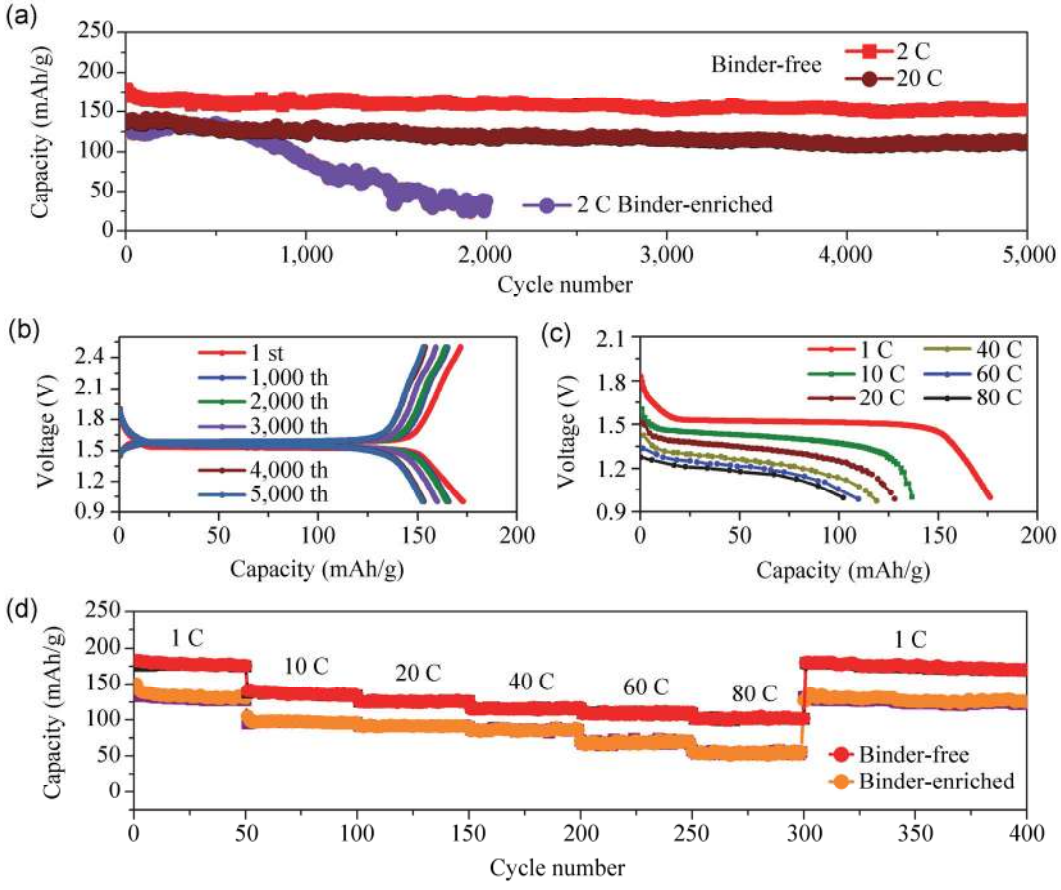

Figure 3 (a) Electrochemical performances of the web-like LTO anode: (a) Long-life cycling performance at 2 C and 20 C, (b) galvanostatic charge–discharge curves at 2 C, and (c) discharge curves ranging from 1 C to 80 C. (d) Specific discharge capacities of the web-like and binder-enriched anodes at various C rates.

with the conventional binder-enriched LTO anode, as revealed in Fig. 3(d). Compared with the binder-enriched electrode, the specific capacities of the binder-free web-like LTO anode are substantially increased at all investigated charge–discharge rates from 1 C to 80 C. For instance, at a rate of 80 C, the web-like LTO architecture exhibited a capacity of 103 $mA{\cdot}h{\cdot}g^{-1}$, about two times greater than that of the LTO nanowire coating on Cu foil. After 300 cycles, the discharge capacity of the LTO nanostructures returned to their original value without degradation, revealing their excellent reversibility. Furthermore, the capacities of the binder-free web-like LTO anode decrease slowly with the increase of rate, illustrating its superior rate performance.

The enhanced lithium-ion storage capacity, cycling performance and improved storage kinetics, particularly at high C rates, of the binder-free electrode can be ascribed to the increased number of active sites, the reduced transport path for ions and electrons due to the 1D nanostructures, and the enhanced contact surface between the electrode material and electrolyte attributed to the 3D architecture. To give more direct evidence, the morphologies of the anode after 500 and 2,000 charge–discharge cycles at 2 C were compared. As can be seen in Fig. 4, there was no significant structural degradation of the LTO nanowires on Ti foil, confirming their excellent morphological stability during the electrochemical reactions, which contributes to the superior electrochemical performances of the binder-free LTO anode. A low-magnification SEM image of the anode after 500 charge–discharge cycles is also given in Fig. S2 (in the ESM) and confirms the structural stability of the LTO nanowires.

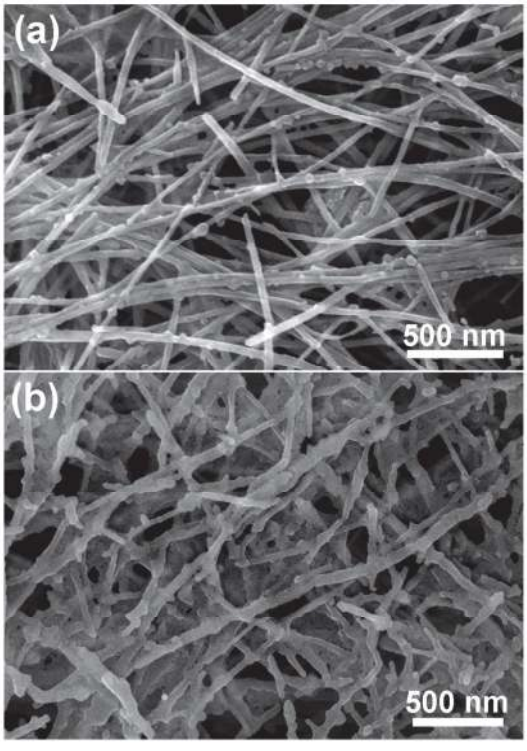

Figure 4 SEM images of the LTO anode after (a) 500 and (b) 2,000 charge–discharge cycles at a current rate of 2 C.

3.3 Flexible full batteries

To explore the potential application of the ultralong-life and high-rate web-like LTO architecture as the anode for a flexible full battery, spinel LMO nanorods were synthesized and selected as the cathode material because of their 3D tunnel structure for the migration of lithium ions and advantage of fast charging resulting from the stable delithiated structure [19, 36–38]. The structures and electrochemical performance of the LMO nanorods are shown in Figs. S3–S6 (in the ESM). Using the LMO nanorods coated on flexible stainless steel cloth, with over-capacity relative to that of LTO anode, as the cathode, a flexible full battery was assembled, and the device structure is shown in Fig. 5(a). The photograph of the full battery with an active area of 3 × 1 cm is shown in Fig. S7 (in the ESM). Figure 5(b) shows the charge–discharge voltage profiles of the as-fabricated LTO half-cell, LMO half-cell and flexible LTO//LMO full-cell, respectively. As expected from the operating voltages of the LTO anode and the LMO cathode, their combination produces a battery with an operating voltage of about 2.4 V.

The cycling performance of the as-fabricated full battery is shown in Fig. 5(c). When tested at low current rate of 2 C, the capacity remains at 168 $mA{\cdot}h{\cdot}g^{-1}$ after 70 charge–discharge cycles, which is even higher than its initial value (163 $mA{\cdot}h{\cdot}g^{-1}$). In addition, the voltage platforms show little change over the whole charge–discharge cycle processes (Fig. 5(d)), demonstrating the excellent stability of the flexible battery. An additional great advantage of the flexible full battery is that the battery can be operated at high C rate, as revealed in Fig. 5(c). The capacity remains at 120 $mA{\cdot}h{\cdot}g^{-1}$ at a high rate of 20 C after 70 cycles, thus retaining about 98% of its initial value. The results demonstrate the outstanding cycling stability of the flexible full battery even at high C rate. More importantly, compared with the capacity at 2 C, there is only a 25% capacity loss at a high current rate of 20 C for the flexible full battery, indicating its superior rate performance.

Real applications of flexible batteries depend on their mechanical properties and stability under various bending conditions. Figures 6(a)–6(c) show the robustness tests of our fabricated flexible battery at different fixed bending states on a bending stage machine. At bending conditions from states 1 to 3 (corresponding to Figs. 6(a)–6(c)), the charge–discharge profiles were recorded during the galvanostatic cycling tests at a rate of 2 C. In the first charge–discharge process, there is only a small capacity loss with increasing bending degree (Fig. 6(d)), and after 60 charge–discharge cycles, the voltage platform under bending states 2 and 3 also suffers from little degradation (Fig. 6(e)), demonstrating the excellent mechanical stability. The cycling performance of the flexible full batteries under bending states 2 and 3 are depicted in Fig. 6(f). The capacities remain at 147 and 133 $mA{\cdot}h{\cdot}g^{-1}$ after 60 cycles, about 93% and 88% of their initial values under bending states 2 and 3, respectively. The reduction in specific capacity can be attributed to the charge transfer of lithium ions from and into the electrode and the contact resistance existing between the anode and cathode, which are greatly affected by residual internal stresses of the flexible battery. After being fully charged, the flexible battery was able to light a blue light-emitting diode (LED) even in the bent state, as shown in Fig. 6(g). The high-rate and outstanding flexibility of the LTO-based full battery make it very

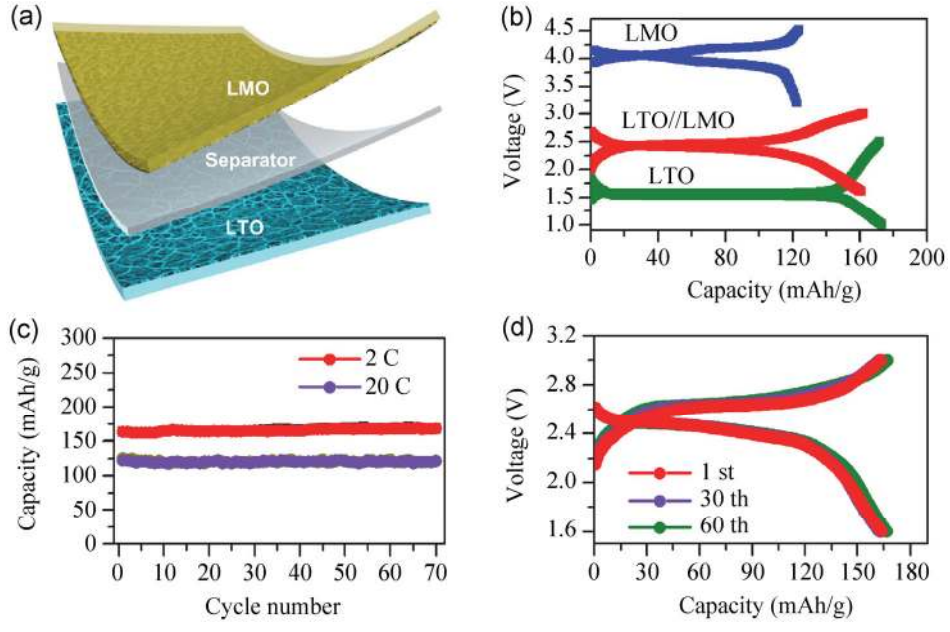

Figure 5 (a) Schematics of the as-fabricated flexible battery. (b) Galvanostatic charge–discharge curves at 2 C of the LMO, LTO half cells and the assembled full battery. (c) Cycling performance at 2 C and 20 C, and (d) charge–discharge curves at 2 C of the full battery.

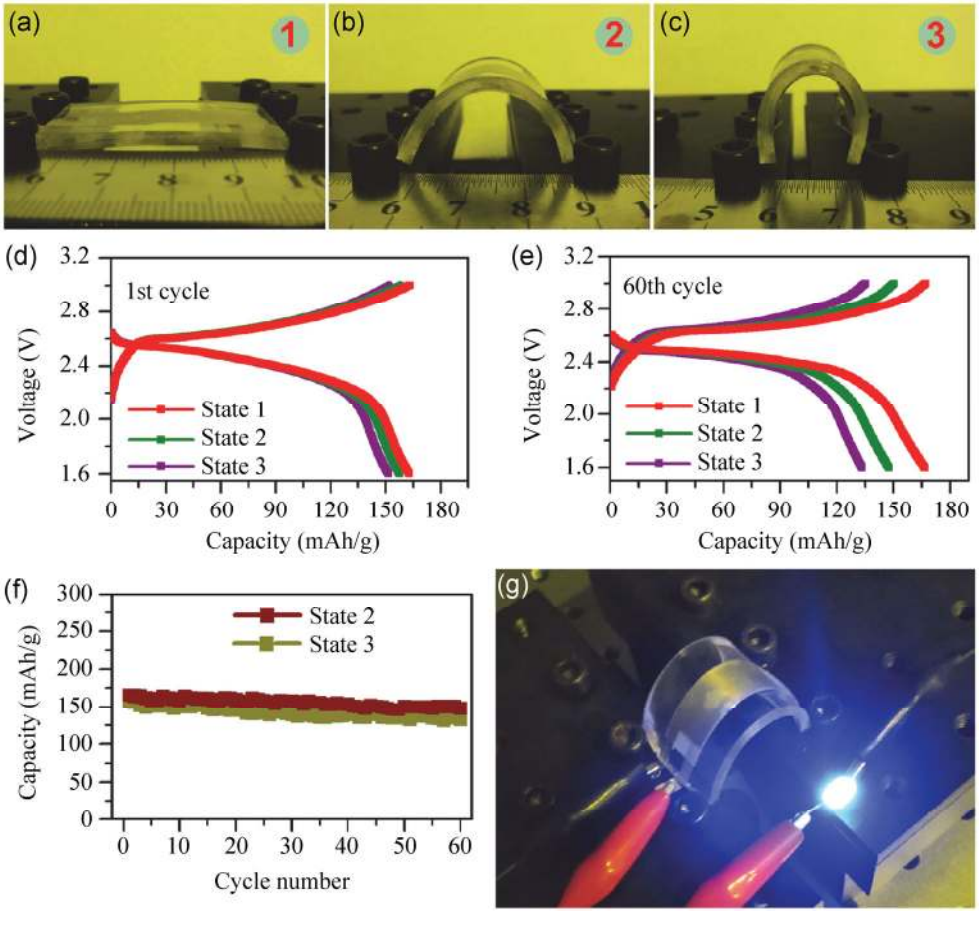

Figure 6 (a)–(c) Photographs of the as-assembled flexible battery at different bending states. Charge–discharge curves of the full battery at different bending states at the (d) 1st cycle and (e) 60th cycle at 2 C. (f) Cycling performance of the battery at state 2 and 3 at 2 C. (g) Lighting a blue LED device under bending.

promising for flexible electronics that require shape-conformability and excellent mechanical properties.

4 Conclusions

A web-like LTO architecture formed by assembly of numerous nanowires on Ti foil has been directly used as the binder-free anode for LIB, and exhibited ultralong life up to 5,000 cycles at 2 C and 20 C without obvious performance degradation, with enhanced rate capabilities at various current rates ranging from 1 C to 80 C compared with the conventional binder-enriched LTO nanowire electrode. The excellent electrochemical performance can be ascribed to the improved number of active sites, reduced transport path for ions and electrons due to the 1D nanowires, and enhanced contact surface between the electrode material and electrolyte attributed to the 3D architecture and binder-free anode. More importantly, a flexible full battery assembled from the binder-free web-like LTO anode and LMO nanorods cathode demonstrated high capacity and cycling stability even at a high current of 20 C, and excellent mechanical stability with acceptable capacity loss under severe bending. The superior flexibility of the battery coupled with its outstanding cycle reversibility, high rate performance, and excellent mechanical stability make it very promising for the next-generation flexible electronics.

Acknowledgements

We acknowledge the support from the National Natural Science Foundation (Nos. 91123008 and 61377033), the 973 Program of China (No. 2011CB933300), the Program for New Century Excellent Talents of the University in China (Grant No. NCET-11-0179), the Fundamental Research Funds for the Central Universities (No. HUST: 2013NY013) and Wuhan Science and Technology Bureau (No. 20122497).

Electronic Supplementary Material: Supplementary material (XPS spectra O 1s and Ti 2p in LTO nanosructures, low-magnification SEM image of the LTO anode, SEM image of the LMO nanorods, photograph, charge–discharge curves, long-life cycling performance of LMO cathode, and photograph of the flexible full battery) is available in the online version of this article at http://dx.doi.org/10.1007/s12274-014-0470-7.

References

[1] Armand, M.; Tarascon, J. M. Building better batteries. *Nature* **2008**, *451*, 652–657.

[2] Wang, X. F.; Liu, B.; Wang, Q. F.; Song, W. F.; Hou, X. J.; Chen, D.; Cheng. Y. –B.; Shen, G. Z. Three-dimensional hierarchical $GeSe_2$ nanostructures for high performance flexible all-solid-state supercapacitors. *Adv. Mater.* **2013**, *25*, 1479–1486.

[3] Pushparaj, V. L.; Shaijumon, M. M.; Kumar, A.; Murugesan, S.; Ci, L.; Vajtai, R.; Ajayan, P. M. Flexible energy storage devices based on nanocomposite paper. *Proc. Natl. Acad. Sci. U.S.A.* **2007**, *104*, 13574–13577.

[4] Nishide, H.; Oyaizu, K. Toward flexible batteries. *Science* **2008**, *319*, 737–738.

[5] Wang, X. F.; Liu, B.; Liu, R.; Wang, Q. F.; Hou, X. J.; Chen, D.; Wang, R. M.; Shen, G. Z. Fiber-based flexible all-solid-state asymmetric supercapacitors for integrated photodetecting system. *Angew. Chem. Int. Ed.* **2014**, *53*, 1849–1853.

[6] Wang, X. F.; Song, W. F.; Liu, B.; Chen, G.; Chen, D.; Zhou, C. W.; Shen, G. Z. High-performance organic–inorganic hybrid photodetectors based on P3HT:CdSe nanowire heterojunctions on rigid and flexible substrates. *Adv. Funct. Mater.* **2013**, *23*, 1202–1209.

[7] Hu, L. B.; Wu, H.; La Mantia, F.; Yang, Y.; Cui, Y. Thin, flexible secondary Li-ion paper batteries. *ACS Nano* **2010**, *4*, 5843–5848.

[8] Hu, L. B.; Choi, J. W.; Yang, Y.; Jeong, S.; La Mantia, F.; Cui, L. F.; Cui, Y. Highly conductive paper for energy-storage devices. *Proc. Natl. Acad. Sci. U.S.A.* **2009**, *106*, 21490–21494.

[9] Liu, B.; Wang, X. F.; Liu, B. Y.; Wang, Q. F.; Tan, D. S.; Song, W. F.; Hou, X. J.; Chen, D.; Shen, G. Z. Advanced rechargeable lithium-ion batteries based on bendable $ZnCo_2O_4$-urchins-on-carbon-fibers electrodes. *Nano Res.* **2013**, *6*, 525–534.

[10] Li, N.; Chen, Z. P.; Ren, W. C.; Li, F.; Cheng, H.-M. Flexible graphene-based lithium ion batteries with ultrafast charge and discharge rates. *Proc. Natl. Acad. Sci. U.S.A.* **2012**, *109*, 17360–17365.

[11] Kwon, Y. H.; Woo, S. W.; Jung, H. R.; Yu, H. K.; Kim, K.; Oh, B. H.; Kim, J. Y. Cable-type flexible lithium ion battery based on hollow multi-helix electrodes. *Adv. Mater.* **2012**,

24, 5192–5197.

[12] Lin, H. J.; Weng, W.; Ren, J.; Qiu, L. B.; Zhang, Z. T.; Chen, P. N.; Chen, X. L.; Deng, J.; Wang,Y. G.; Peng, H. S. Twisted aligned carbon nanotube/silicon composite fiber anode for flexible wire-shaped lithium-ion battery. *Adv. Mater.* **2014**, *26*, 1217–1222.

[13] Koo, M.; Park, K. I.; Lee, S. H.; Suh, M.; Jeon, D. Y.; Choi, J. W.; Lee, K. J. Bendable inorganic thin-film battery for fully flexible electronic systems. *Nano Lett.* **2012**, *12*, 4810–4816.

[14] Xu, S.; Zhang, Y. H.; Cho, J.; Lee, J.; Huang, X.; Jia, L.; Fan, J. A.; Su, Y.; Su, J.; Zhang, H. G., et al. Stretchable batteries with self-similar serpentine interconnects and integrated wireless recharging systems. *Nat. Commun.* **2013**, *4*, 1543.

[15] Choi, K.-H.; Cho, S.-J.; Kim, S.-H.; Kwon, Y. H.; Kim, J. Y; Lee, S. -Y. Thin, deformable, and safety-reinforced plastic crystal polymer electrolytes for high-performance flexible lithium-ion batteries. *Adv. Funct. Mater.* **2014**, *24*, 44–52.

[16] Yu, L.; Wu, H. B.; Lou, X. W. Mesoporous $Li_4Ti_5O_{12}$ hollow spheres with enhanced lithium storage capability. *Adv. Mater.* **2013**, *25*, 2296–2300.

[17] Liu, S. H.; Wang, Z. Y.; Yu, C.; Wu, H. B.; Wang, G.; Dong, Q.; Qiu, J. S.; Eychmüller, A.; Lou, X. W. A flexible TiO_2 (B)-based battery electrode with superior power rate and ultralong cycle life. *Adv. Mater.* **2013**, *25*, 3462–3467.

[18] Luo, J. S. ; Liu, J. L.; Zeng, Z. Y.; Ng, C. F.; Ma, L. J.; Zhang, H.; Lin, J. Y.; Shen, Z. X.; Fan, H. J. Three-dimensional graphene foam supported Fe_3O_4 lithium battery anodes with long cycle life and high rate capability. *Nano Lett.* **2013**, *13*, 6136–6143.

[19] Wang, X. F.; Xiang, Q. Y.; Liu, B.; Wang, L. J.; Luo, T.; Chen, D.; Shen, G. Z. TiO_2 modified FeS nanostructures with enhanced electrochemical performance for lithium-ion batteries. *Sci. Rep.* **2013**, *3*, 2007.

[20] Zhu, G. N.; Liu, H. J.; Zhuang, J. H.; Wang, C. X.; Wang, Y. G.; Xia, Y. Y. Carbon-coated nano-sized $Li_4Ti_5O_{12}$ nanoporous micro-sphere as anode material for high-rate lithium-ion batteries. *Energy Environ. Sci.* **2011**, *4*, 4016– 4022.

[21] Zhang, G. Q.; Wu, H. B.; Hoster, H. E.; Chan-Park, M. B.; Lou, X. W. Single-crystalline $NiCo_2O_4$ nanoneedle arrays grown on conductive substrates as binder-free electrodes for high-performance supercapacitors. *Energy Environ. Sci.* **2012**, *5*, 9453–9456.

[22] Zhou, X. S.; Cao, A. M.; Wan, L. J.; Guo, Y. G. Spin-coated silicon nanoparticle/graphene electrode as a binder-free anode for high-performance lithium-ion batteries. *Nano Res.* **2012**, *5*, 845–853.

[23] Luo, J. S.; Xia, X. H.; Luo, Y. S.; Guan, C.; Liu, J. L.; Qi, X. Y.; Ng, C. F.; Yu, T.; Zhang, H.; Fan, H. J. Rationally designed hierarchical TiO_2@Fe_2O_3 hollow nanostructures for improved lithium ion storage. *Adv. Energy Mater.* **2013**, *3*, 737–743.

[24] Wang, X. F.; Liu, B.; Xiang, Q. Y.; Wang, Q. F.; Hou, X. J.; Chen, D.; Shen, G. Z. Spray-painted binder-free SnSe electrodes for high-performance energy-storage devices. *ChemSusChem*, **2014**, *7*, 308–313.

[25] Wang, Y. Q.; Gu, L.; Guo, Y. G.; Li, H.; He, X. Q.; Tsukimoto, S.; Ikuhara, Y. C.; Wan, L. J. Rutile-TiO_2 nanocoating for a high-rate $Li_4Ti_5O_{12}$ anode of a lithium-ion battery. *J. Am. Chem. Soc.* **2012**, *134*, 7874–7879.

[26] Shen, L. F.; Uchaker, E.; Zhang, X. G.; Cao, G. Z. Hydrogenated $Li_4Ti_5O_{12}$ nanowire arrays for high rate lithium ion batteries. *Adv. Mater.* **2012**, *24*, 6502–6506.

[27] Shen, L. F.; Ding, B.; Nie, P.; Cao, G. Z.; Zhang, X. G. Advanced energy-storage architectures composed of spinel lithium, metal oxide nanocrystal on carbon textiles. *Adv. Energy Mater*. **2013**, *3*, 1484–1489.

[28] Chen, S.; Xin, Y.; Zhou, Y. L.; Ma, Y. R.; Zhou, H. H.; Qi, L. M. Self-supported $Li_4Ti_5O_{12}$ nanosheet arrays for lithium ion batteries with excellent rate capability and ultralong cycle life. *Energy Environ. Sci.* **2014**, *7*, 1924–1930.

[29] Kim, J. G.; Shi, D.; Park, M. S.; Jeong, G.; Heo, Y. U.; Seo, M.; Kim, Y. J.; Kin, J. H.; Dou, S. X. Controlled Ag-driven superior rate-capability of $Li_4Ti_5O_{12}$ anode for lithium rechargeable battery. *Nano Res.* **2013**, *6*, 365–372.

[30] Ma, Y.; Ding, B.; Ji, G.; Lee, J. Y. Carbon-encapsulated F-doped $Li_4Ti_5O_{12}$ as a high rate anode material for Li^+ batteries. *ACS Nano* **2013**, *7*, 10870–10878.

[31] Zhao, L.; Hu, Y. S.; Li, H.; Wang, Z. X.; Chen, L. Q. Porous $Li_4Ti_5O_{12}$ coated with N-doped carbon from ionic liquids for Li-ion batteries. *Adv. Mater.* **2011**, *23*, 1385–1388.

[32] Chen, X. B.; Liu, L.; Peter, Y. Y.; Mao, S. S. Increasing solar absorption for photocatalysis with black hydrogenated titanium dioxide nanocrystals. *Science* **2011**, *331*, 746–750.

[33] Wang, G. M.; Wang, H. Y.; Ling, Y. C.; Tang, Y. C.; Yang, X. Y.; Fitzmorris, R. C.; Wang, C. C.; Zhang, J. Z.; Li, Y. Hydrogen-treated TiO_2 nanowire arrays for photoelectrochemical water splitting. *Nano Lett.* **2011**, *11*, 3026–3033.

[34] Etacheri, V.; Yourey, J. E.; Bartlett, B. M. Chemically bonded TiO_2-bronze nanosheet/reduced graphene oxide hybrid for high-power Li-ion batteries. *ACS Nano* **2014**, *8*, 1491–1499.

[35] Song, T.; Han, H.; Choi, H.; Lee, J. W.; Park, H.; Lee, S.;

Park, W. I.; Kim, S.; Liu, L.; Paik, U. TiO_2 nanotubes branched tree on carbon nanofiber nanostructure as an anode for high energy and power lithium ion batteries. *Nano Res.* **2014**, *7*, 491–501.

[36] Hosono, E.; Kudo, T.; Honma, I.; Matsuda, H.; Zhou, H. Synthesis of single crystalline spinel $LiMn_2O_4$ nanowires for a lithium ion battery with high power density. *Nano Lett.* **2009**, *9*, 1045–1051.

[37] Xiao, X. L.; Lu, J.; Li, Y. D. $LiMn_2O_4$ microspheres: Synthesis, characterization and use as a cathode in lithium ion batteries. *Nano Res*. **2010**, *3*, 733–737.

[38] Xiao, X. L.; Wang, L.; Wang, D. S.; He, X. M.; Peng, Q.; Li, Y. D. Hydrothermal synthesis of orthorhombic $LiMnO_2$ nano-particles and $LiMnO_2$ nanorods and comparison of their electrochemical performances. *Nano Res*. **2009**, *2*, 923–930.